Doppler Shifting Technique for Generating Multi-Frames of Video SAR via Sub-Aperture Signal Processing

Chul Ki Kim, Muhammad Tayyab Azim, Ashish Kumar Singh, *Member, IEEE*, and Seong-Ook Park, *Member, IEEE*

***Abstract*—The signal processing technologies of synthetic aperture radar (SAR) have been vastly studied as diverse measurement modes for various applications. One of the technologies is Video-SAR (ViSAR). It is a land-imaging mode where a sequence of images is continuously formed on the spotlight mode. We propose a new signal processing method to generate the multi-frames of ViSAR using Doppler shifting technique via sub-aperture processing. The method is based on our designed wide-angle antenna, which is a corrugated horn shape with low side lobe and Gaussian beam pattern. This wide-angle antenna receives a wide Doppler band along the azimuth direction. Based on the characteristics of the antenna, we separate the wide Doppler band into each chirp pulse signal. Each of these separated signals has a different center time. Through each chirp pulse signal in Doppler domain, the proposed method generates each frame of video at a high frame rate. The proposed ViSAR processing can show high efficiency with low computation and without a fixed coordinate system. Moreover, it can also visualize a wider area on stripmap mode than the conventional ViSAR mode, and can derive the video results based on Range Doppler Algorithm (RDA). These advantages can lead to reduce economic costs and simplify the operating ViSAR system. We have performed the practical experiments using X-band chirp pulse SAR system mounted on an airplane to verify the proposed method.**

***Index Terms*—Airborne SAR, Sub-aperture processing, ViSAR, Wide Angle Antenna, Doppler shifting technique.**

I. Introduction

In ORDER to overcome the disadvantages of optical surveillance system, which is greatly influenced by climate changing and the brightness of light, SAR has been studied as a solution for accurate detection. The reason is that SAR is able to monitor the area of interest throughout day and night under all weather conditions. In addition, the SAR can be diversely applied depending on the purpose, such as a stripmap mode (or standard mode), a spotlight mode (or high-resolution mode), a scan mode, enhanced mode, etc. In the recent research of SAR, ViSAR has been studied for monitoring the area of interest and moving target detection in real-time. In contrast to the conventional SAR image, which focuses on a specific area at a time, ViSAR shows the video image using SAR measurement along the sequential time. Moreover, ViSAR is mostly used to sense a scene of interest while the airborne radar platform is either flying by or circling it in spotlight mode [5], [13], [19], [20]. An airborne radar platform for ViSAR is widely used in military service and space science fields. It is the most effective method than other SAR platforms (e.g., automobile, satellites) in scouting and detecting the area of interest in the air without the restriction of movement.

One of the method for ViSAR processing is to generate sub-apertures for producing frames of video with a fixed coordinate system [31]. Sub-aperture in ViSAR have the advantage to avoid the duplication of signal processing in each frame and hence it reduces the computation complexity. And it can be applied into diverse fields by finding the information of the signal in the sub-aperture [17], [18], [29]. However, there still requires an enormous amount of computation to generate all frames, as the number of scenes in video increases. In order to arrange the continuous frames of ViSAR from sub-aperture, all of frames are constructed with the same resolution and image quality based on a fixed coordinate system such as the common ground output coordinate system (GOCS) [5] and local output coordinate system (LOCS) [3], [5]. The coordinate system is also used for SAR imaging process in range-Doppler domain, which is verified between the scene center and the aperture center with range direction. However, there are still some issues and additional process [22], [23] to be supplemented in geometric correction for consecutive images [26], [27]. Moreover, ViSAR systems form an image in a fixed ground coordinate system and provide feasibility and flexibility with arbitrary flight formation by applying back-projection (BP) algorithm. It has the advantage of persistent sub-aperture processing [18], [20]. However, BP algorithm requires the large amount of computation overhead in SAR signal processing due to the azimuth-wise interpolation loops and pixel-wise accumulation loops therein. To overcome the disadvantage of general BP algorithm, fast back-projection (FBP) [19]–[21], [24] and fast-factorized back-projection (FFBP) [25] have been studied for simple and efficient signal processing.

Manuscript received February 10, 2020; revised May 27, 2020; accepted June 25, 2020. Date of publication July 2, 2020; date of current version July 14, 2020. The associate editor coordinating the review of this manuscript and approving it for publication was Dr. Gang Li. This work was supported in part by the Institute for Information & communications Technology Promotion (IITP) grant funded by the Korea government (MSIT) under grant 2018-0-01658, and in part by the Key Technologies Development for Next Generation Satellites) *(Corresponding author: Chul Ki Kim.)*

The authors are with the School of Electrical Engineering, Korea Advanced Institute of Science and Technology, Daejeon 34141, South Korea (e-mail: chulki@kaist.ac.kr; tayyabazim@kaist.ac.kr; ashish@kaist.ac.kr; soparky@kaist.ac.kr).

Digital Object Identifier 10.1109/TSP.2020.3006749

In this paper, we have proposed a new signal processing method to generate the frames of ViSAR on airborne SAR platform, using the multi-segment application without a fixed coordinate system, i.e. Doppler shifting technique. In other words, we separate the received Doppler frequency band of each chirp pulse signal by the shifted windowing technique. To obtain more frames in the proposed method, it is advantageous that SAR raw data have a wide Doppler band along the azimuth direction. Therefore, we design a wide-angle antenna, which has a Gaussian-beam pattern with low side lobes. In general, the azimuth and range data are neither processed nor compressible in the frequency domain without an arrangement of each frame. However, we apply this method to extract the frames for ViSAR only by separating the received Doppler band and it shows that each frame has a different center time [34], which indicates the time order of the video image. In addition, the results can be generated without a fixed coordinate system in each frame. It also leads to a high frame rate of ViSAR. In other words, the proposed method offers a convenient signal processing with a high frame rate as compared to other conventional methods [5], [12], [18], [20]. This method executes a multi-frame signal processing, based on a Range Doppler Algorithm (RDA). Although the conventional RDA uses a serial process, we improve it to the parallel process for the proposed ViSAR signal processing. And RDA can reduce the amount of computation as compared to BP algorithm for ViSAR. While the required operation number of traditional BP algorithm is proportional to N^3 [20], traditional RDA requires the amount of $5N$. It can lead to increase speed and be a better approach to implementing real-time processing technology in future work. To verify our proposed method, we have performed experiments using an airborne X-band radar system to obtain ViSAR raw data. With the benefit of wide scanning and multi-segment of Doppler shifting technique on an airplane platform, we were able to arrange successive frames along the azimuth direction, called as time-sequential images [2]. To that end, we have proposed a new frame construction for ViSAR, which is a shifting the Doppler window from sup-apertures and improve the efficiency and performance of the signal processing. Moreover, the proposed method has the advantages that we can obtain ViSAR in an easy-to-use stripmap mode, which is standard operating SAR mode. And also, we can apply it to real-time observation with a small amount of computation which can achieve reducing economic costs with minimizing the constraints of the target frequency band. Thus, reducing the burden on hardware system design.

This paper organized as follows. Section II introduces the fundamental theory of RDA processing for SAR. Section III provides a new frame construction scheme for ViSAR on airplane platform. Section IV presents the processed results to verify the proposed technique in the practical experiment with the designed wide-angle antenna. Finally, we demonstrate the conclusions for the proposed method in Section V.

II. SAR Signal Analysis Model in RDA

The RDA is one of the methods to compress a SAR raw data using the matched filters of the range direction and azimuth direction. As shown in Fig. 1, RDA has been used in a stripmap mode with chirp pulse signals. The basic signal processing of RDA consists of range and azimuth compressions, and range cell migration (RCM), as shown in Fig. 2. The estimation method of Doppler signal can also be applied to obtain high-resolution images in SAR experiment. Although the image quality caused by the Doppler frequency variation is insignificant for the ground experiment (Automobile-SAR), it is critical to estimate the accurate Doppler frequency in the case of airborne and spaceborne SAR. The reason is that fast measurement speed and large distance from the target to radar cause an inaccurate change in Doppler chirp band [1]. Therefore, it is important to estimate Doppler chirp pulse signal, using the magnitude and phase information of received signal from the algorithm such as average cross-correlation coefficient (ACCC), multi-look cross-correlation (MLCC) and multi-look beat frequency (MLBF) [1], [2]. The received chirp pulse signals in the range and azimuth directions, respectively, are described as follows:

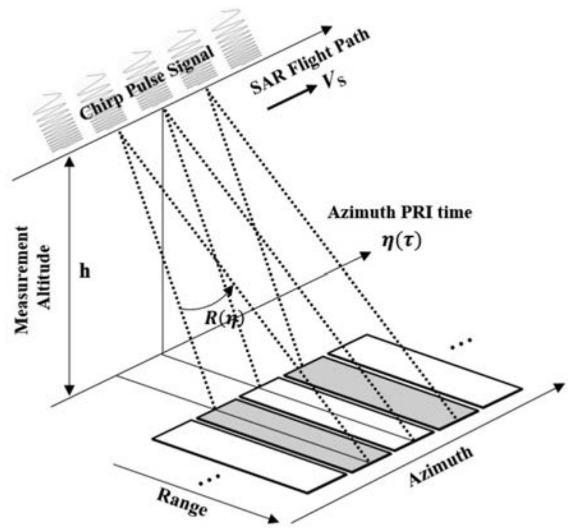

Fig. 1. Airborne-SAR flight mode for chirp pulse radar.

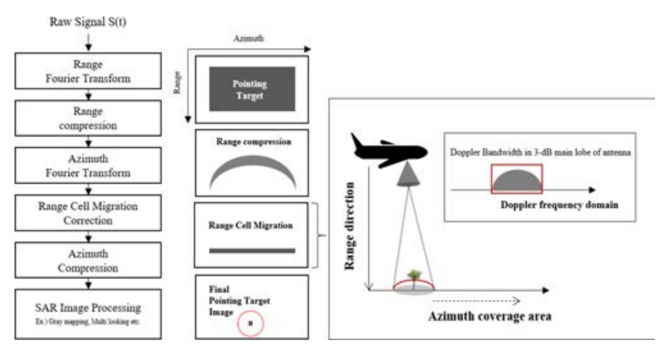

Fig. 2. Conventional Range Doppler Algorithm.

$$S_{range}(\tau,\eta) = A_r\omega_r\left[\tau - \frac{2R(\eta)}{c}\right] e^{\frac{j4\pi f_0 R(\eta)}{c}} e^{j\pi K_r\left[\tau-\frac{2R(\eta)}{c}\right]^2} \tag{1}$$

$$S_{azimuth}(\tau,\ \eta) = A_a\omega_a(\eta-\eta_c)\, e^{j2\pi f_{\eta c}(\tau)} e^{j\pi K_a(\tau)\eta^2} \tag{2}$$

where, τ and η are the range and azimuth time, respectively. ω_r and ω_a are the window functions of each chirp pulse signals, A_r and A_a are the amplitude, f_0 and f_{η_c} are the center frequency of chirp pulse signal, and K_r and K_a are the chirp rate of the signal. In the previous sentence, subscript *r* and *a* stand for range and azimuth direction, respectively. $R(\eta)$ in (1) is the instantaneous slant range. For the range matched filter, the system parameters such as center frequency and chirp rate of pulse signal are used to compress the raw data in the range direction. Likewise, after RCM of SAR data, the performance of resolution for the matched filter in azimuth direction can be determined according to K_a and f_{η_c}. Hence, based on RDA signal processing [1], the final SAR image signal, $S_{final}(\tau,\eta)$ is derived as follows:

$$S_{final}\left(\tau,\eta\right) = A_0 p_r\left(\tau - \frac{2R_0}{c}\right) p_a\left(\eta\right) e^{\left(-j\frac{4\pi f_0 R_0}{c}\right)} e^{j2\pi f_{\eta c}\eta} \tag{3}$$

where, R_0 is the distance of the first signal in range-direction. As an airplane platform for SAR, the errors of the matched filter in azimuth direction are vulnerable by the SAR measurement environment such as actual speed, changing rate in distance from the radar to target, and motion vibrating conditions. Whereas, the matched filter of range direction is verified accurately from the transmitted system parameter and the loop-back chirp pulse signal. Therefore, it is more important to estimate the accurate 'matched filter' in the azimuth direction (Doppler direction) than the range direction. In other words, accurate estimation results lead to the high quality of the video frames from the received Doppler band. For this reason, we focus on the accurate estimation method to obtain a clear ViSAR image from a wide-Doppler band.

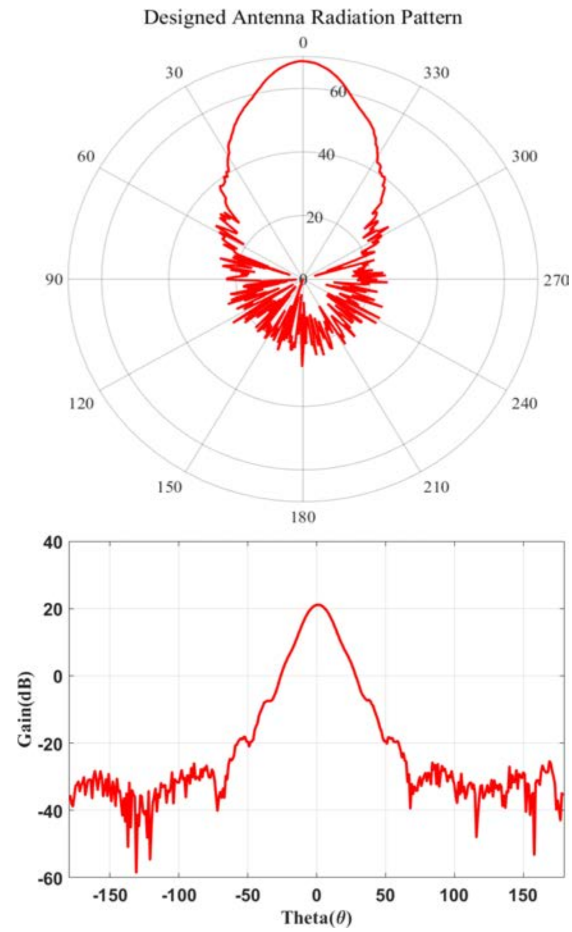

Fig. 3. The radiation pattern of the proposed antenna for wide-angle at X-band.

III. Proposed ViSAR Generation Scheme Through Multi-Segment Application

This section describes the proposed technique that is well suited in ViSAR signal processing. The conventional ViSAR creates the video image using a type of BP algorithm in spotlight mode with a coordinate system and sorted raw data in chronological order. In this paper, we generate the multi-segment frames of ViSAR by estimating Doppler parameters and applying them to Doppler shifting technique. It is operated on RDA while the radar platform is flying by side looking at the scene. To demonstrate our proposed process, we will explain the overall process of technology at III-A. And then, at III-B, the important mathematical Doppler formation in received data is analyzed before understanding the proposed method. At III-C, we describe the generation method of the final ViSAR image processing, based on the analysis of III-B.

A. Overall Progress of Proposed Method

Different from the conventional processing method for ViSAR, we present a modification of the RDA algorithm suitable for ViSAR. To apply this modified RDA in ViSAR, the first step is to fabricate a wide-angle antenna as shown in Fig. 3. This antenna is properly designed to have a wider beam angle with low side level than a conventional SAR antenna. In SAR processing, the total beam angle of antenna is related to the resolution of an image, quadratic phase error, and interference of unexpected signal. Therefore, the narrow beam angle of antenna improves the performance of SAR processing in general. However, this type of antenna has limitations in narrowing the measurement range and producing multiple scenes of ViSAR. In this work, we have generated multiple frames using an antenna with a wide beam angle, by utilizing its wide Doppler band. The following sections B and C will introduce how to generate the frames in detail. Therefore, we designed a new antenna with a wide-angle and low side lobe to minimize the disadvantage of a general wide-angle antenna. In particular, our designed antenna can receive clear Doppler information, since the low side lobe level reduces the interference from an unexpected direction. In addition, it causes expanding the available angle of aperture due to low sidelobe gain. Fig. 3. shows the radiation pattern of the proposed antenna. Thus, the raw data, which have various Doppler information from a wide-angle antenna, can be processed to multiple frames for the video image. Fig. 4 illustrates the phenomenon caused by the expansion of the antenna beam angle. In a squint mode, Doppler bandwidth from the antenna can be described as follows [1]:

$$\Delta f_{dop} = \left|\frac{2V_s\cos\theta_s}{\lambda}\theta_{bw}\right| \tag{4}$$

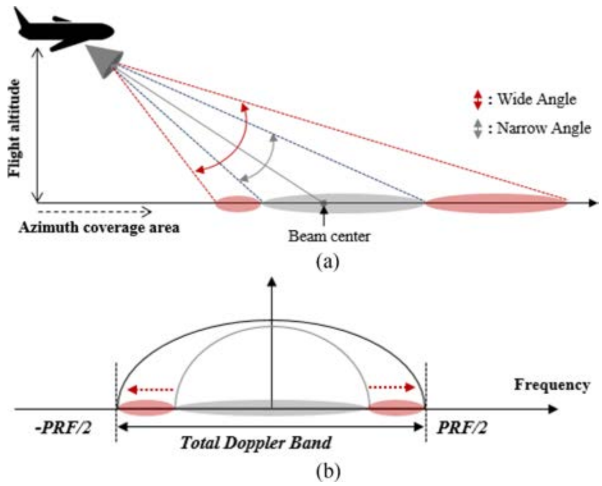

Fig. 4. Geometry of airborne-SAR with wide-angle antenna.

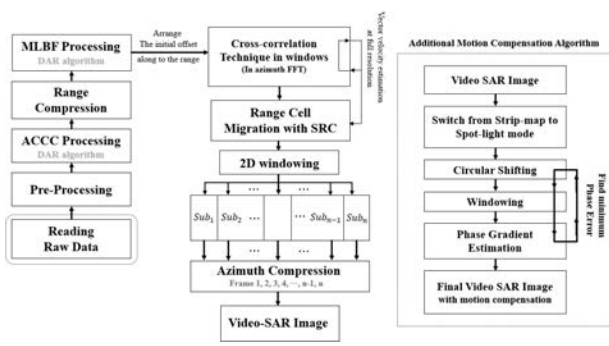

Fig. 5. Block diagram of the Proposed ViSAR algorithm based on RDA.

where θ_{bw} is the 3-dB width of the antenna beam width, θ_s is squint angle for measuring the target, *Vs* is the velocity of the measurement platform and λ is the wavelength of center frequency in the chirp pulse signal. Equation (4) indicates that the expansion of the antenna beam width can be proportional to the wide Doppler frequency band. Thus, to utilize the received data from a wide-angle antenna, we need to study an accurate Doppler estimation method to separate the wide Doppler band as one of the segments for the frame of ViSAR. In our case, Doppler data are received as several superimposed chirp pulse signals because of the wide reception range of the antenna, shown as Fig. 6(a). Therefore, we need to apply an accurate estimation algorithm for the separation of the received Doppler data along each azimuth direction. Accurate estimated Doppler parameters become an important foundation to generate the frames of video in our proposed method. Among the various Doppler estimation methods, we utilize the modified ACCC and MLBF algorithm with the weighted window for generating each sub-frames. For this reason, in the received signals by our wide-angle antenna, Doppler chirp pulses can be represented by the sum of equation (2) in the azimuth direction, shown as (5):

$$s_{azimuth}\left(\tau,\ \eta\right)=\sum_{n=1}^{m}A_a\omega_a\left(\eta-\eta_c\right)e^{j2\pi f_{\eta_c}(\tau,n)}e^{j\pi K_a(\tau,n)\eta^2} \tag{5}$$

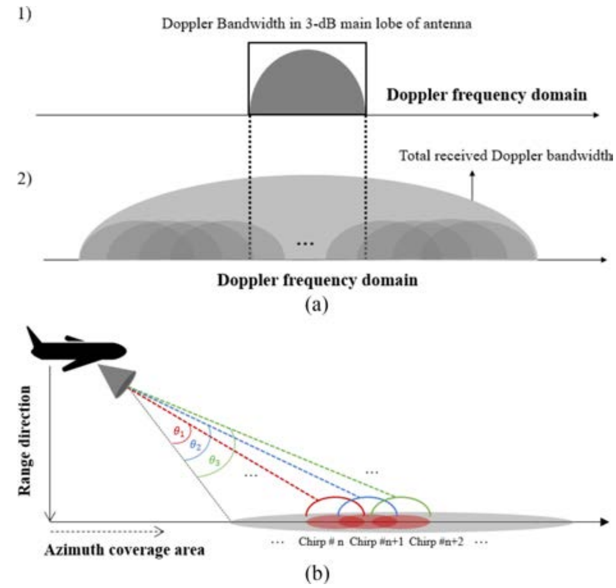

Fig. 6. (a) The characteristics of received bandwidth 1) from the conventional antenna and 2) the proposed antenna with wide-angle, (b) the separated chirp signals in wide-angle of antenna.

where, '*n*' is the Doppler chirp number along the azimuth direction and η_c is the beam center offset time. Doppler chirp pulse signal is approximate as exponentials based on the Doppler centroid frequency and Doppler Chirp rate. As the squint angle of antenna changes, the relative range of the radar and target on the same platform also changes. Thus, the Doppler centroid frequency and the Doppler chirp rate are defined in (6) along the azimuth direction, respectively. Also, in Fig. 6(b), we illustrate the picture of Doppler chirp signals through a wide-angle antenna.

$$f_{\eta_c}\left(\tau,n\right)=\frac{2V_s\sin\left(\theta_{s(n)}\right)}{\lambda},K_a\left(\tau,n\right)\cong\frac{2V_s^2\cos^3\theta_{s(n)}}{\lambda R_0\left(\tau\right)}$$
$$n=1,2,3,4,\cdots(shift\ order\ along\ the\ azimuth\ direction) \tag{6}$$

where, $R_0(\tau)$ is the slant range along the range sample time. These parameters are important to explain the multi-segment application method for generating the frames of ViSAR. In other words, each Doppler chirp pulse signal generates each frame of video through the Doppler shifting technique. Fig. 2 and Fig. 6 show the analysis difference between the conventional method and the proposed method. We will describe the detailed generation process in Section III-B and III-C. Additionally, considering the residual phase error in the estimated Doppler information, the cross-correlation technique [6]–[8] is applied for the compensation in each frame. After finishing the compensation, we propose the modified process of RCM and azimuth compression, based on the Doppler information. To help in understanding the overall process, the proposed RDA algorithm is shown in Fig. 5. After this section, we will introduce the formulations of the method in Fig. 5, called Doppler shifting technique, in detail to demonstrate the enhanced performance.

B. Doppler Formulation for ViSAR imaging

As mentioned above, one of the important points in the proposed technique is to estimate and arrange each Doppler frequency within the whole aperture of a wide-angle antenna. This Section III-B is important to lead the parameters for the azimuth-matched filter in the part of azimuth compression. Therefore, as shown in Fig. 5, there are 8 steps before dividing into a number of frames of ViSAR.

1) **Pre-Processing**: removing the interference signals caused by transmitting and receiving antennas.
2) **ACCC Processing**: estimating Doppler centroid frequency of each sub-aperture based on the modified ACCC algorithm.
3) **Range Compression**: convolution between raw data and range matched filter.
4) **MLBF Processing**: Measuring the ambiguity of Doppler frequency through the modified MLBF algorithm.
5) **Cross-correlation Technique**: Compensating the residual phase error in each Doppler chirp signal by cross-correlation technique.
6) **Range Cell migration with SRC**: Range phase interpolation with a squint-angle through RCM.
7) **2D windowing & Azimuth Compression**: Convolution the received Doppler signals with azimuth matched filters along the azimuth angle in each sub-aperture.
8) In addition, **the phase gradient algorithm (PGA)** is added in the case, the motion compensation is required due to the unexpected measurement environment.

We estimate the Doppler parameters (by [2])the modified ACCC and [3])MLBF) so that raw-data is separated into each frame of ViSAR after [3])Range compression. And, based on these estimated parameters, the process of generating a ViSAR image will be described in [7])Azimuth Compression. Steps 1), 5), 6) and 8) are the additional procedures required to obtain high-quality SAR images. Thus, we focus on how to generate the frames of ViSAR in the proposed multi-frame signal processing as follow.

First, as shown in Fig. 6(a), the received signal is constructed by the sum of the Doppler frequencies in a wide aperture of the antenna:

$$s\left(\tau,\eta\right) = A\omega_r e^{\frac{j4\pi f_0 R(r,\eta)}{c}} e^{j\pi K_r\left[\tau-\frac{2R(r,\eta)}{c}\right]^2}\sum_n \omega_n e^{j2\pi f_{\eta_c}(\tau,n)} e^{j\pi K_a(\tau,n)\eta^2} \tag{7}$$

We use a squinted equivalent range model in (7) to reduce the error of relative distance between radar and target [9], [14]–[16]. The total slant ranges for Doppler band between airplane and target in each sub-aperture can be expressed as

$$R\left(r,\eta\right) = \sum_n \sqrt{r^2 + \left(V\eta\right)^2 - 2rV\eta\cos\theta_n} \tag{8}$$

where *r* is the distance between the sub-aperture center and target, θ_n is the corresponding equivalent squint angle, *V* is the equivalent speed of an radar platform. Based on equation (7), Doppler centroid frequency can be estimated by the ACCC algorithm in the 2D-FFT domain. ACCC algorithm is one of the developed methods for estimating the Doppler centroid frequency. The advantage of the ACCC algorithm is that it can estimate the phase difference without phase wrapping problem [1]–[4]. The ACCC formulation is defined as the sum of the correlation between two successive azimuth signals from raw data. Since our designed antenna receives a wide Doppler band, we estimated each center frequency of each interval in Doppler domain. We construct the weighted signal in case of subsampled data, as our main concept:

$$s_n\left(\eta\right) = \mathrm{IFFT}\left[\mathrm{window}_n\left\{\mathrm{FFT}\left(\mathrm{s}\left(\eta\right)\right)\right\}\right] \quad \left(n = \theta_1, \theta_2, \ldots, \theta_{\mathrm{n}-1}\theta_{\mathrm{n}}\right) \tag{9}$$

Each weighted signal by the window can be estimated at the respective center frequency by the ACCC algorithm. In addition, the interference of the overlapping signals can be minimized due to the windowing sized by the calculated Doppler bandwidth [1].

Therefore, the ACCC algorithm, as follows (10), expresses the correlation phase of the weighted signals:

$$\sum_n \phi_{accc,n} = \frac{d\phi\left(\eta\right)}{d\eta}\Big|_{\eta=\eta_1,\eta_2,\eta_3\cdots\eta_n}\Delta\eta$$

$$\sum_n f'_{\eta_{c,n}} = \frac{PRF}{2\pi}\sum_n \phi_{accc,n}$$

$$\left(n = \theta_1, \theta_2, \ldots, \theta_{\mathrm{n}-1}\theta_{\mathrm{n}}\right) \tag{10}$$

where f'_{η_c} is baseband Doppler centroid frequency and *PRF* indicates abbreviation of 'Pulse Repetition Frequency'. $\Delta\eta$ is a sampling interval, ϕ_{accc} is the average phase increment, wrapped within the interval $(-\pi, +\pi]$. Some results of the estimated Doppler centroid frequency are shown as the orange line in Fig. 7(a), which has an ambiguous signal. These ambiguous signals occur when the frequency is generated beyond the bandwidth of PRF. Therefore, after range compression, we estimate the ambiguity number to recover the exact signals by MLBF algorithm [1], [2], [4], [11], [12]. In the proposed method, we need to modify the MLBF algorithm of FFT type [10] to estimate the accurate ambiguity number in frequency domain.

$$\sum_n f_{absolute,\eta_{c,n}} = -\sum_n \frac{f_0}{\Delta f_r} f_{beat,n}$$

$$\left(n = \theta_1, \theta_2, \ldots, \theta_{\mathrm{n}-1}\theta_{\mathrm{n}}\right) \tag{11}$$

where $f_{absolute,\eta_c}$ is absolute Doppler centroid frequency, Δf_r is a look size of chirp pulse bandwidth and f_{beat} is the beat frequency from the MLBF algorithm. Processing MLBF algorithm, we determine the parameters of the received signals to introduce a beat frequency in equation (11). One of the parameters is the cutoff look size of the signal. It needs to define the size of a weighted windowing, considering the interference of the surrounding signals. The power of the interested chirp signal is similar to the unexpected peripheral signals. It leads inaccuracy to estimate the beat frequency. Thus, we guard the target signal with windowing from the interference of the unexpected peripheral signals. Based on experimental data, this study estimates the beat frequency after 1) setting the look size to near the peak energy and 2) cover the weighting function in each look of chirp. The final step in the modified MLBF algorithm, it chooses the significantly high magnitude sample to estimate

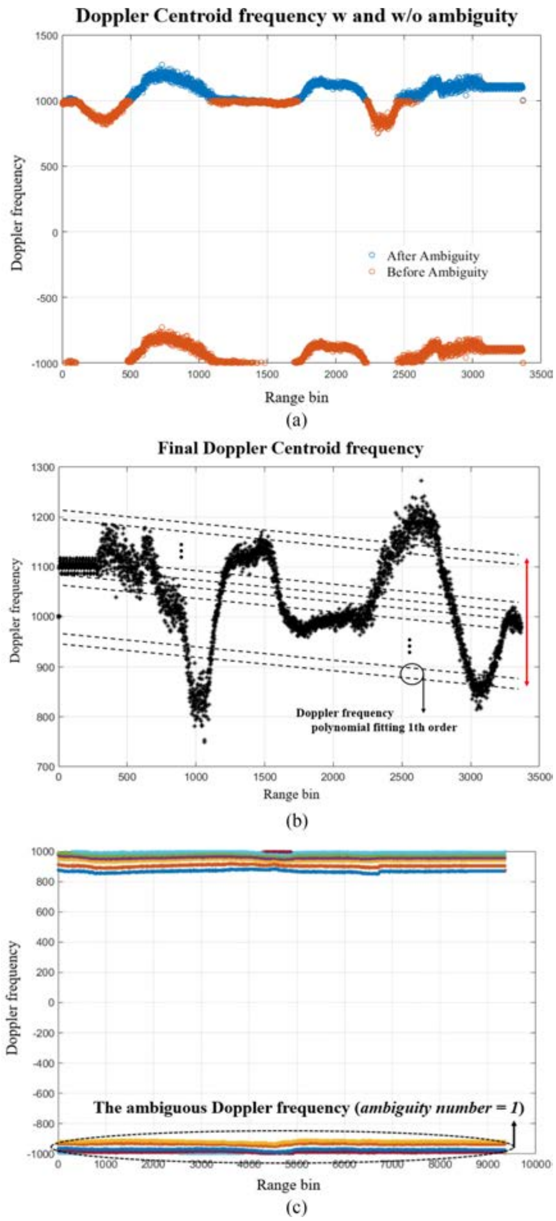

Fig. 7. The result of Doppler centroid frequency from ACCC algorithm in the measured data of practical experiment. (a) Comparison with and without ambiguity, (b) Doppler centroid frequency after ACCC and MLBF processing, and (c) Configuration of estimated Doppler signals with windowing in the aperture of a wide-angle antenna.

the beat frequency. Fig. 8(a) and (b) show the results between the conventional MLBF and the proposed MLBF, respectively. It is clear that the beat frequency estimated by the modified MLBF algorithm is a more accurate result than the conventional MLBF algorithm. Doppler ambiguity number is determined by the difference between baseband Doppler centroid frequency and absolute Doppler centroid frequency [1]. Based on these results, we can arrange the exact Doppler centroid frequency in each chirp pulse band as follow:

$$\sum_n f_{\eta_{c,n}} = \sum_n \left(f'_{\eta_{c,n}} + M_{amb,n} PRF \right) \quad (n = \theta_1, \theta_2, \cdots, \theta_{\mathrm{n-1}}\theta_{\mathrm{n}}) \tag{12}$$

where f_{η_c} is Doppler centroid frequency of chirp pulse band, M_{amb} is ambiguity number. To analyze the above equation, we exploit the actual experimental raw data that will be verified in the next section. Fig. 7(a) demonstrates that the estimation process as shown by the blue line can recover accurate Doppler centroid frequency. In Fig. 7(b), the estimated Doppler value without the windowing shows a large deviation of 450 Hz, which varies from 800 to 1250 Hz. The large deviation decreases the quality of SAR image through RCM, secondary range compression (SRC), and azimuth compression. Therefore, based on our main concept, superimposed Doppler chirp pulse signals can be estimated, having a deviation of about 20 Hz in the bandwidth between 850 and 1250 Hz as shown in Fig. 7(c). In other words, the estimated Doppler centroid frequencies of each chirp pulse signal are obtained by shifting the window through the polynomial fitting as shown in Fig. 7(b) and (c). In this section, we show each Doppler band from the superimposed signals from a wide-angle antenna to generate frames of ViSAR. Fig. 9 shows one of the frames in ViSAR, comparing the results with/without our proposed method. For the above reason, it leads to large Doppler variation and each frame of ViSAR cannot be focused accurately. Thus, the wide Doppler band can be separated into the exact several bands. The estimated Doppler signals are defined from (6) to the following equation:

$$\begin{aligned} & f_{\eta_{c(total)}}(\tau) \\ & = f_{\eta_c}(\tau,\theta_1) + f_{\eta_c}(\tau,\theta_2) + \cdots + f_{\eta_c}(\tau,\theta_{n-1}) + f_{\eta_c}(\tau,\theta_n) \\ & = \sum_n f_{\eta_c}(r,\theta_n) \\ & n = 1,2,3,4,\ldots(shift\ order\ along\ the\ azimuth\ direction) \end{aligned} \tag{13}$$

where, θ_n is the beam angle in the wide-beam antenna, as shown in Fig. 6(b). Based on the accurate Doppler centroid estimation, it also requires to apply the exact Doppler chirp rate, $K_a(\tau, n)$ under variable environmental conditions [3]–[5]. It leads the expected resolution of each frame of video, using the azimuth-matched filter that fits with each Doppler chirp pulse signal. Shown as (6), the velocity of the airplane (V_s) is one of the key parameters to introduce the Doppler parameters. Therefore, we need to find accurate velocity in Doppler parameters to increase the quality of SAR images. In this method, the incident velocity in each Doppler band is different because each Doppler band has a different incident angle of the antenna. In other words, the correction of velocity is necessary to improve image quality for each frame. To find the accurate Vs, the proposed algorithm includes a cross-correlation technique for estimation Doppler chirp rate in each frame. If $S(\tau, \eta)$ is a 2-D signal constructed in range and azimuth, the cross-correlation function is defined as follows [7], [8].

$$(s_{Look1} * s_{Look2})(\tau_n, \eta) \underline{\mathrm{def}} \int_{-\infty}^{\infty} s^*_{Look1}(\tau_n) s_{Look2}(\tau_n, \eta + \omega)\, d\omega \quad (n = 1,2,3,4,\ldots, maximum\ range\ cell)$$

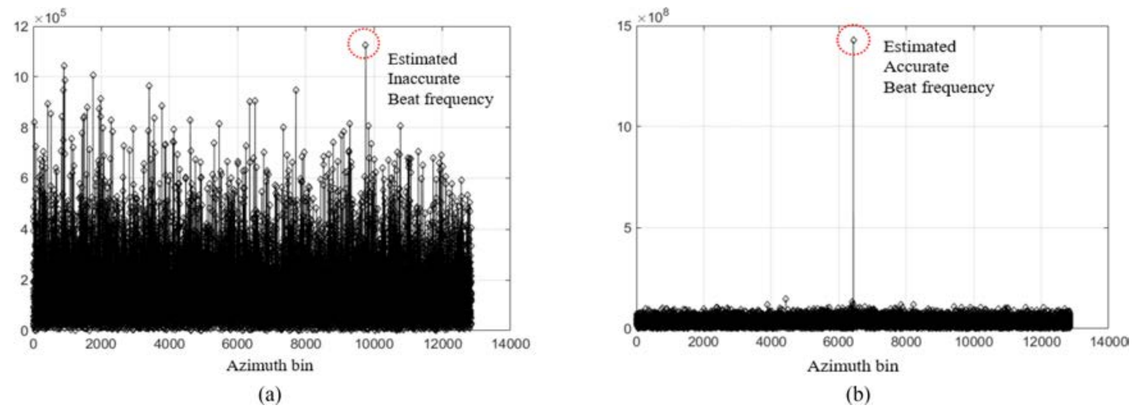

Fig. 8. Estimation of beat frequency in azimuth plane from overlapped Doppler band. (a) The conventional MLBF and (b) the proposed MLBF.

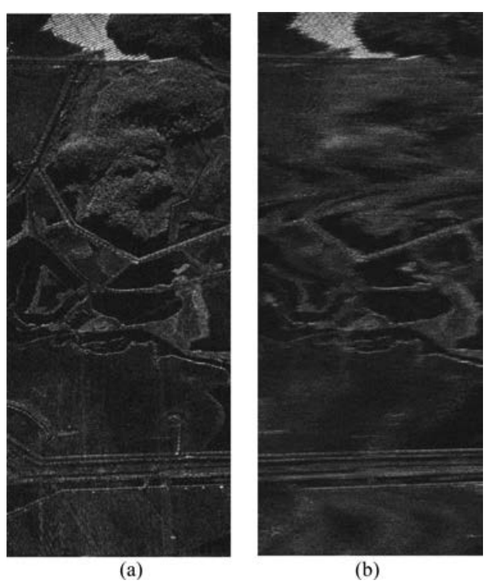

Fig. 9. Output frame of ViSAR using (a) accurate and (b) inaccurate Doppler parameter estimation.

After the range compression, the cross-correlation function divides the chirp pulse frequency into two looks (look-1 and look-2) based on the Doppler centroid frequency. These looks have different phase information, having $V_s + \Delta V_{error}$ [33]. To compensate for this phase difference, the cross-correlation values between the two looks are compared until the smallest correlation value is reached. The modification of velocity in each range line optimizes the cross-correlation value to remove ΔV_{error}. The final estimated V_s can be variable over a range, such as a vector component. RCM, SRC and azimuth compression are performed by the Doppler parameters from the result of the cross-correlation estimation.

In the next step, we introduced how the estimated Doppler information in a wide-angle angle of antenna is arranged in the time sequence of video and how to calculate the azimuth-matched filters, which produce the frames of ViSAR based on the estimated Doppler parameters. Finally, we will generate the final ViSAR image via the proposed technique in detail.

C. ViSAR Imaging Process

After the Doppler estimation process to separate each chirp pulse signals in the azimuth frequency band, we propose a way to generate frames of ViSAR along the azimuth direction. Fig. 10 shows the principle and process for video frames according to the antenna beam angle. In Fig. 10(a), the elapsed time between the radar and target is proportional to the angle of an antenna in wide beam width. It means that the angle of the antenna (from ϑ_1 to ϑ_2) increases the elapsed time (t_1 to t_2) along the azimuth direction. Thus, considering this phenomenon, the Doppler parameters in equation (6) can also be redefined as a function, which varies with time:

$$\begin{aligned} f_{\eta_c}(\tau) &= \sum_n f'_{\eta_c}(r, \theta(t_n)) = \sum_n \frac{2V_s \sin(\theta(t_n))}{\lambda}, \\ K_a(\tau, n) &\cong \frac{2V_s^2 \cos^3\theta(t_n)}{\lambda R_0(\tau)} \\ &\qquad n = 1,\ 2,\ 3,\ 4,\ \cdots (shift\ order) \end{aligned} \tag{14}$$

By this concept, the Doppler centroid frequency, which varies with angle, follows the time sequence. Besides, the range equation of RCM (14) and the form of cross-coupling of SRC (16) must be calculated with Doppler frequency changes, considering a high order model caused by the high squint [1]. These processes help to get high-quality images of the squinted raw data. It is also the time-ordered equations as shown below:

$$\sum_n R_{rd}(f_\eta(t_n)) - R_0 = R_0 \sum_n \left[\frac{1 - D(f_\eta(t_n), V_r(\tau))}{D(f_\eta(t_n), V_r(\tau))} \right] \tag{15}$$

$$H_{src}(f_\tau) = \sum_n e^{-j\pi \frac{f_\tau^2}{K_{src}(R_0, f_\eta(t_n))}} \tag{16}$$

To generate the sub-images of ViSAR, the azimuth-matched filters for each Doppler chirp pulse signal are derived as shown in the following equation:

$$H_{azimuth}(f_\eta, t_n) = \sum_n e^{j \frac{4\pi R_0(\tau) D(f_\eta(t_n), V_r(\tau)) f_c}{c}} \tag{17}$$

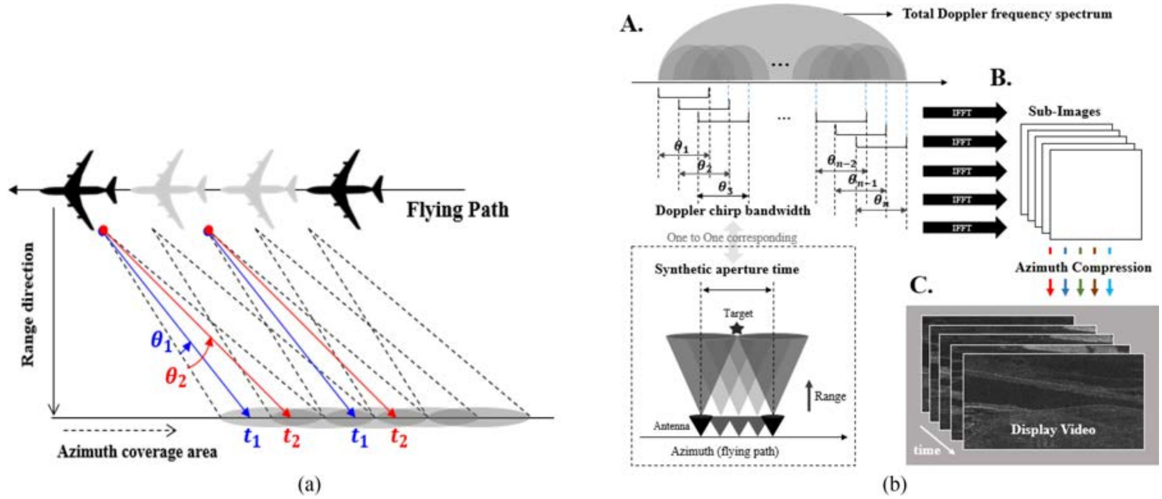

Fig. 10. (a) The elapsed time from the airplane to ground according to the angle (b) the process structure after the Doppler estimation.

where, f_η is Doppler frequency, f_c is the center frequency and c is light speed, and $D(f_\eta(t_n), V_r(\tau))$ is migration factor in high-squint mode [1]. The convolution between the processed signals and the azimuth-matched filters generate each desired scene in time-order. It means that each Doppler chirp signal is separated by the azimuth-compression. Thus, it produces continuous frames of a video with a time sequence according to the angles because each frame has a different elapsed time [34]. To help understand the process, we describe the process of generating frames in Fig. 10(b). As it makes Doppler chirp bands according to the beam angles, we can separate them from the total received Doppler frequency spectrum. Overlapped Doppler chirp pulse bands in Part A are signal-processed into the sub-images of Part B according to the angles of sub-aperture in antenna. After part B, each sub-image produce frames of ViSAR, through azimuth-compression. Under the results of part B, we can reconstruct the frames as a continuous display. Continuous display of images in Part C indicates ViSAR in the observed area. In the end, we can apply the phase compensation algorithm, called PGA [35], to minimize the phase error of the received signal. However, in the verification experiment, PGA cannot show a significant difference in the results because of the stable measurement conditions in the airplane. Thus, this paper focuses on the analysis of the proposed ViSAR frame generation method. Nevertheless, a phase compensation algorithm is necessary at a higher resolution SAR image and unstable measurement environment.

In addition, analyzing the final results, we can also determine the frame rate of ViSAR by our proposed concept as follow:

$$Frame\ rate = \gamma_n \sigma_{res} \left| \frac{2V_s \cos\theta_s}{\lambda} \right| \theta_{bw} \frac{1}{T_0} \tag{18}$$

where γ_n is the overlapping number, σ_{res} is azimuth resolution and T_0 is the exposure time of target in a wide-angle antenna. θ_{bw} is a beam width that can be received by the antenna used in the ViSAR experiment. The frame rate of (18) indicates how many images can be generated in the area of interest for a second, shown as Fig. 11. In the proposed multi-segment method, the frame rate is proportional to how many frames are overlapped at the target during the exposure time (T_0). Azimuth resolution is a parameter that determines the interval between overlapped Doppler bands. Moreover, it is also very important how much the antenna for ViSAR can receive the signals from the target. In our experiment, we can generate the high-frame rate (5Hz at X-band in the airborne platform) in the desired wide band based on the proposed method. It has a higher result than the frame rate calculated by a typical equation in [5], [32] (2 Hz at X-band in the same condition of the airborne platform). From these results of the overall process, the proposed technique can derive video SAR images efficiently at a high frame rate without a fixed coordinate system.

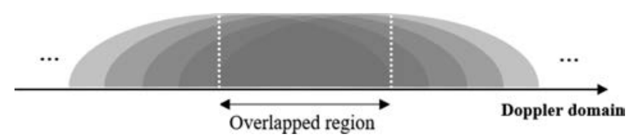

Fig. 11. The overlapped Doppler region for the area of interest.

IV. Experiment and Results

To evaluate the proposed algorithm, the X-band SAR system is designed for the practical experiment. The X-band radar system is commonly used for military and government systems. We carried out the experiments on an airplane to observe the terrain in the Republic of Korea such as fields, sea, and mountains. Table I shows the specifications of the X-band SAR system for the measurement of ViSAR. Based on the system, we cover a 1.7 km in stripe range line by one-pixel resolution (0.5 m). Simultaneously, each range resolution of a target is supported by 0.75 m resolution. In azimuth direction, a one-pixel resolution is 0.042 m and each azimuth resolution is supported by 0.15 m.

As shown in Fig. 12, two antennas are installed, one is for the transmitter and the other is for the receiver, respectively. The stop-and-go method produces the azimuth frames of a ViSAR image. To prove the validity of the proposed technique in the

TABLE I
X-BAND SAR SYSTEM SPECIFICATION

System Parameter	Value
Airplane Model	Citation jet 1+c525
Center Frequency	9.65 GHz
Chirp signal Bandwidth	200MHz
Range/Azimuth Resolution	0.75m/0.15m
Chirp pulse duration	20 μsec
PRF	2000 Hz
Operating mode	Stripmap
Airplane Velocity	< 320 km/h
Flying height	< 1.5 km
Squint angle	≈ 7°
Look angle	70° ∼ 75°
Overall angle of antenna	30°
Polarization	Single-Pol (Linear)

Fig. 12. The picture of SAR measurement setup: (a) Airplane appearance, (b) inside view, and (c) outside view.

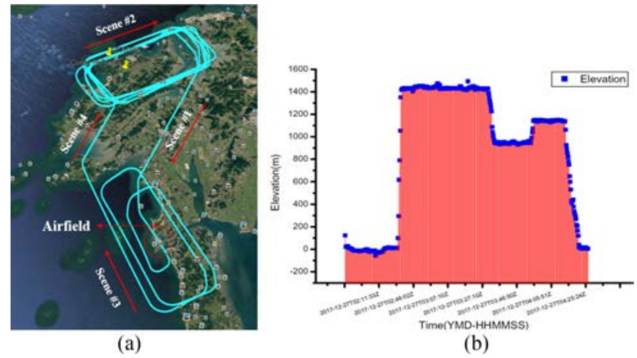

Fig. 13. (a) Flying path and (b) Flying height in practical experiment.

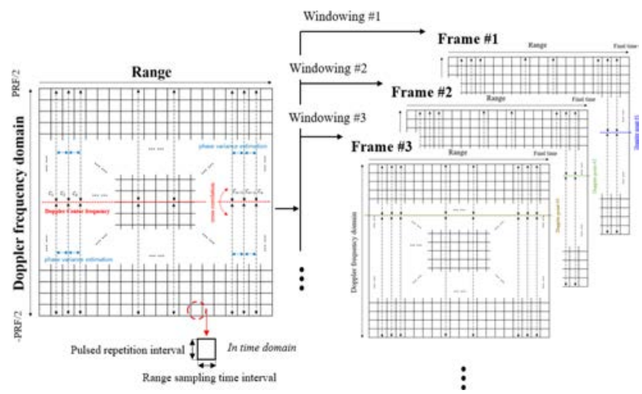

Fig. 14. Received raw data cube from the X-band SAR system.

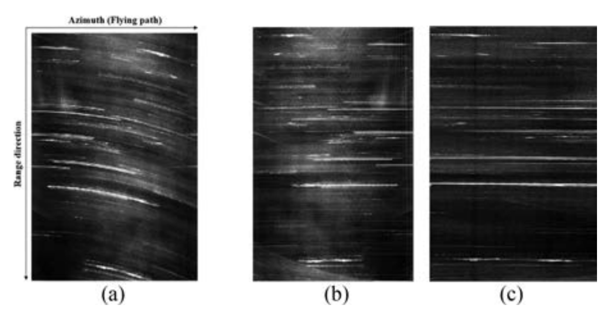

Fig. 15. (a) The SAR data in time domain after range compression, (b) Range-Doppler domain, and (c) time domain after RCMC, respectively.

diverse experiments, we obtain the data at the flying height of 1 km, 1.2 km and 1.5 km for 1 hour and record the airplane route by GPS, illustrated in Fig. 13(a) and (b), respectively. Scene #1 and #2 are places to fly through the rice field and small mountains, Scene #3 is the airfield, which has the moving components and Scene #4 is the place for solar power plant. The measured raw data of scene #1, #2, #3 and #4 are clear evidence that the proposed method is valid for ViSAR processing.

After reviewing for missing signals in the received data, the designed SAR system arranges and preprocesses the raw data according to the format to decrease the noise. The received raw data cubes are described in Fig. 14. The raw data consist of 18753 samples in each pulse and 17504 azimuth pulses. The data, used for the proposed method, can be arranged uniformly without any missing samples. For accurate signal processing, the proposed algorithm should be applied after converting it to a range-Doppler domain. Then, Fig. 15(a) shows that the high squint angle of antenna tilts the raw data after RC. Fig. 15(b) in Doppler domain and (c) in time domain show the results of compensating the squint phase through RCM and SRC based on the proposed ACCC and MLBF algorithm. Finally, through azimuth compression with the matched filters for each sub-frames, we produce the outcome of ViSAR images as shown in Fig. 16. It leads 5Hz frame rate in each video scene. As seen in Fig. 16(a)–(d), it can be confirmed that the scenery in the area of interest moves according to the time order. Since the radar reproduces the actual observation in real time, we can observe the area of interest in the video. Particularly from Fig. 17(a) to (e), moving components in the white circle line can be observed

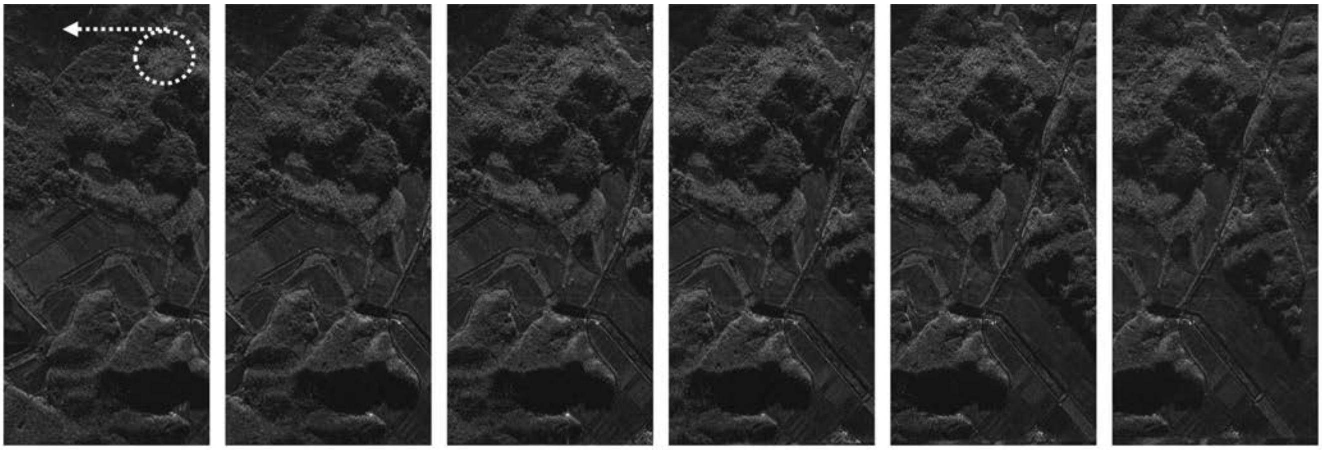

(a)

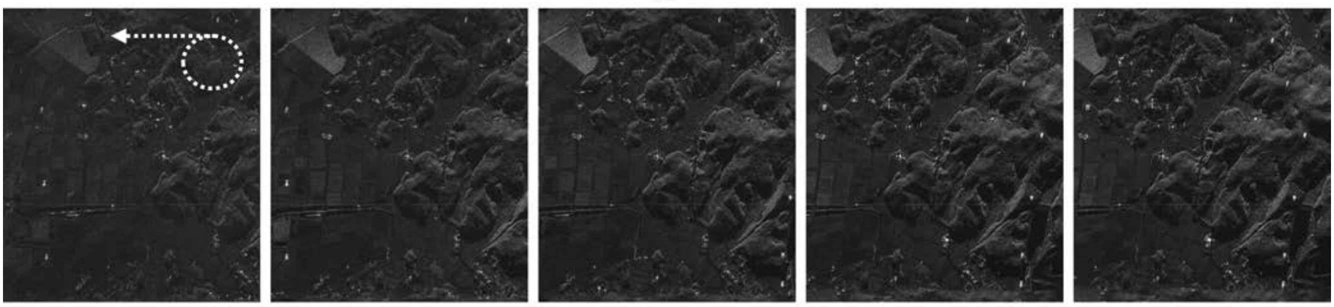

(b)

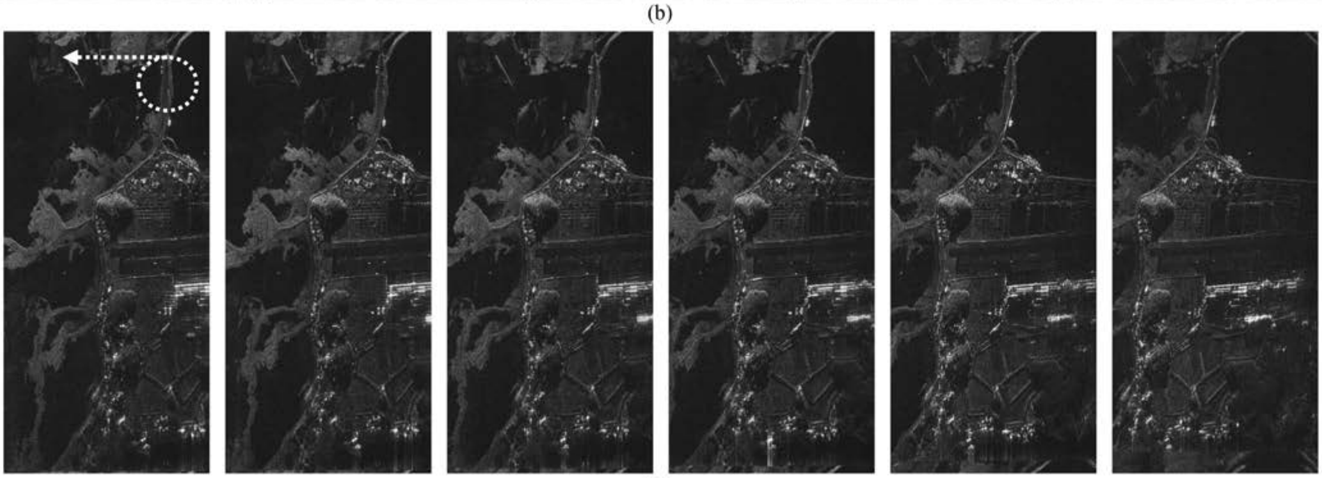

(c)

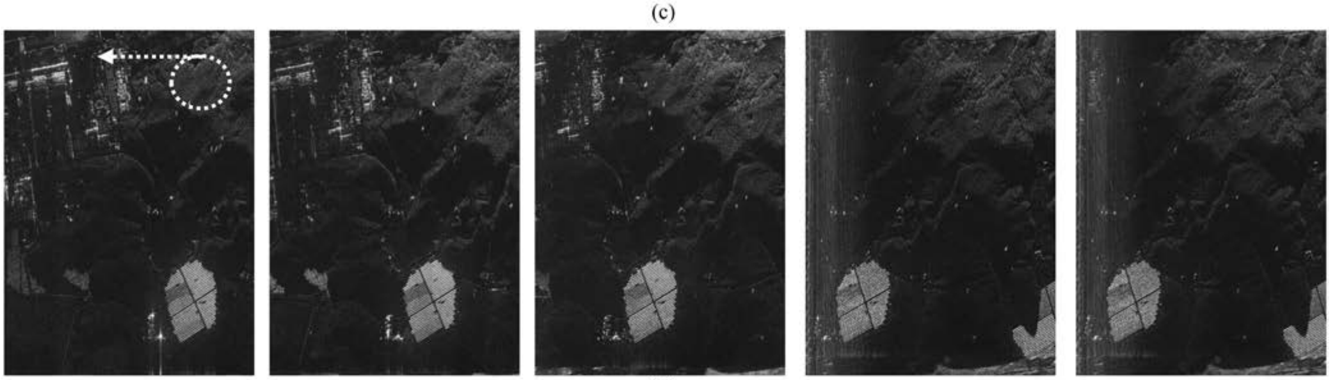

(d)

Fig. 16. Final Video SAR image (5Hz frame rate): (a) Mountains and fields #1, (b) Mountains and fields #2, (c) Airfield #3, and (d) Solar power plant #4 in Taean-gun, Republic of Korea.

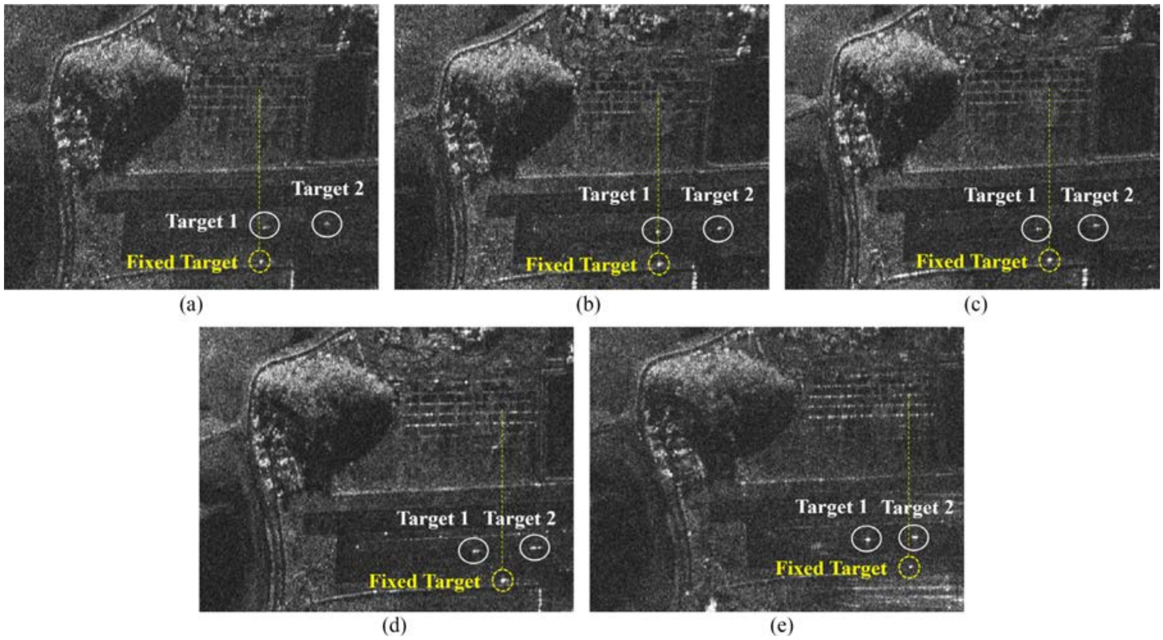

Fig. 17. The moving components in scene #3 (a) frame #1, (b) frame #13, (c) frame # 34, (d) frame #55, and (e) frame #90.

on the flight road of scene #3. Since each separated Doppler chirp signal has a different center time, we can monitor the moving targets whose position changes [34]. Along with each Doppler signals, we can not only obtain a video of SAR image but also detect moving targets. However, if a moving target moves more than a certain speed compared to the SAR radar, a more advanced algorithm is needed to detect it [34]. In future work, we will improve the proposed method for a moving target, based on a single channel GMTI algorithm [29], [30]. To summarize the results so far, the proposed method on RDA can generate the video images at a high frame rate and observe the moving targets in an easy and less complex manner than other conventional ViSAR techniques.

V. Conclusion

In this paper, we propose a new signal processing method to generate focusing frames of ViSAR on the airborne platform through the multi-segment application of Doppler shifting technique within wide Doppler bandwidth. The proposed technique introduces the Doppler parameter estimation and Doppler shifting technique to generate the frames of ViSAR. The proposed focusing algorithm can work with a wide-angle antenna, which can receive wide Doppler bandwidth. Since the wide Doppler bandwidth has diverse information, we can also monitor the wide area of interest along the azimuth direction. For multiple processing of Doppler centroid frequencies, Doppler parameters are utilized to construct the sub-frames in parallel through the azimuth-matched filters. Based on the proposed Doppler method, it is easy to handle and generate the images of video at a high frame rate with low complexity and stable performance without a fixed coordinate system. Moreover, we can apply it in real-time ViSAR signal processing as implementing ViSAR without changing mode or operating system. This process can reduce the burden on the hardware system and the iterative work, which makes each frame of video. Finally, we can obtain clear video SAR images and observe the wide-interested area than conventional spotlight mode. In addition, the real data experiment also verifies the feasibility of this method in practice. The combination of ViSAR and multi-segment application of Doppler shifting technique with a wide-angle antenna could make the synergy, which is attractive for an advanced ViSAR. And, it can be applied even on other SAR platforms (e.g., automobile, satellite) and various operation mode (e.g., spotlight, enhanced, scanSAR mode, etc.). In line with the global trend of miniaturized satellites (CubeSat, MicroSat, etc.), this paper suggests the possibility of developing a cheap cost & small size system by applying the proposed signal processing. For further research, the proposed method should be applied on GMTI for the Doppler shifting technique to obtain the more accurate shape of moving components in the frames of ViSAR.

References

[1] I. G. Cumming and F. H. Wong, *Digital Processing of Synthetic Aperture Radar Data*. London, U.K.: Artech House Inc., 2005.
[2] J. C. Curlander and R. N. McDonough, *Synthetic Aperture Radar Systmes and Signal Processing*. NewYork, NY, USA: Wiley, 1991.
[3] S. Norvang, “Estimating the Doppler centroid of SAR data,” *IEEE Trans. Aerosp. Electron. Syst.*, vol. 25, no. 2, pp. 134–140, Mar. 1989.
[4] S. Li, “Improved doppler centroid estimation algorithm for satellite SAR data,” M.S. thesis, Dept. Elect. Comp. Eng., British Columbia Univ., Vancouver, CAN, 2005.
[5] R. Hu, R. Min, and Y. Pi, “A video-SAR imaging technique for aspect-dependent scattering in wide angle,” *IEEE Sensors J.*, vol. 17, no. 12, pp. 3677–3688, Jun. 2017.
[6] Y. Tang, C. Wang, H. Zhang, and Y. He, “An auto-registration method for space-borne SAR images based on FFT-shift theory and correlation analysis in multi-scale scheme,” in *Proc. IEEE Int. Geosci. Remote Sens. Symp.*, 2013, pp. 3550–3553.
[7] Y. Yue, X. Zhang, and S. Jun, “Motion compensation method for Translational Variant Bistatic SAR using auto-correlation variance,” in *Proc. IET Int. Radar Conf.*, 2009, pp. 1–4.

[8] K. Ouchi and Seong-In Hwang, "Improvement of ship detection accuracy by SAR multi-look cross-correlation technique using CFAR," in *Proc. IEEE Int. Geosci. Remote Sens. Symp.*, 2010, pp. 3716–3719.
[9] J. B. Wang, "Refined ECS Algorithm for high-resolution spaceborne spotlight SAR data processing," in *Proc. Asia Pacific Radio Sci. Conf.*, 2004, pp. 250–253.
[10] S. Li and I. Cumming, "Improved beat frequency estimation in the MLBF doppler ambiguity resolver," in *Proc. IEEE Int. Geosci. Remote Sens. Symp.*, 2005, pp. 3348–3351.
[11] B. C. Sew, Y. K. Chan, and C. S. Lim, "Modified multilook cross correlation (MLCC) algorithm for Doppler centroid estimation in synthetic aperture radar signal processing," *Prog. Electromagn. Res. C*, vol. 20, pp. 215–225, 2011.
[12] T. Yamaoka, K. Suwa, "Radar video generated from synthetic aperture radar image," in *Proc. IEEE Int. Geosci. Remote Sens. Symp.*, 2016, pp. 6509–6512.
[13] A. Damini and B. Balaji, "A videoSAR mode for the x-band wideband experimental airborne radar," in *Proc. SPIE Proc.: Algorithms Synthetic Aperture Radar Imagery XVIII*, 2010, Paper 76990E.
[14] Y. Wang, J.-W. Li, and J. Chen, "A parameter-adjusting polar format algorithm for extremely high squint SAR imaging," *IEEE Trans. Geosci. Remote Sens.*, vol. 52, no. 1, pp. 640–650, Jan. 2014.
[15] M. Xing, Y. Wu, and Y. D. Zhang, "Azimuth resampling processing for highly squinted synthetic aperture radar imaging with several modes," *IEEE Trans. Geosci. Remote Sens.*, vol. 52, no. 7, pp. 4339–4352, Jul. 2014.
[16] G. Wang, L. Zhang, and Q. Hu, "A novel range cell migration correction algorithm for highly squinted SAR imaging," in *Proc. CIE Int. Conf. Radar*, Oct. 2016.
[17] Y. Sun, X. Jing, S. Sun, and H. Huang, "The Subaperture secondary range compression algorithm for near space squint SAR," in *Proc. IEEE Int. Symp. Signal Process. Inf. Technol.*, Dec. 2013, pp. 338–343.
[18] J. Miler, E. Bishop, and A. Doerry, "An application of back projection for video SAR image formation exploiting a subaperture circular shift register," *Proc. SPIE*, vol. 8746, Apr. 2013, Art. no. 874609.
[19] E. Bishop, R. Linnehan, and A. Doerry, "Video-SAR using higher order Taylor terms for differential range," in *Proc. IEEE Radar Conf.*, Philadelphia, PA, USA, May 2016, pp. 1–4.
[20] X. Song and W. Yu, "Processing video-SAR data with the fast back projection method," *IEEE Trans. Aerosp. Electron. Syst.*, vol. 52, no. 6, pp. 2838–2848, Dec. 2016.
[21] A. F. Yegulalp, "Fast backprojection algorithm for synthetic aperture radar," in *Proc. IEEE Radar Conf.*, Waltham, MA, USA, Apr. 1999, pp. 60–65.
[22] H. S. Stone, M. T. Orchard, E.-C. Chang, and S. A. Martucci, "A fast direct Fourier-based algorithm for subpixel registration of images", *IEEE Trans. Geosci. Remote Sens.*, vol. 39, no. 3, pp. 760–776, Jul. 2003.
[23] S. Leprince, S. Barbot, F. Ayoub, and J. P. Avouac, "Automatic and precise orthorectification, coregistration, and subpixel correlation of satellite images, application to ground deformation measurements", *IEEE Trans. Geosci. Remote Sens.*, vol. 45, no. 6, pp. 1529–1558, Jun. 2007.
[24] P. O. Frolind and L. M. H. Ulander, "Evaluation of angular interpolation kernels in fast back-projection SAR processing," *IEE Proc.-Radar, Sonar Navigat.*, vol. 153, no. 3, pp. 243–249, Jun. 2006.
[25] L. M. H. Ulander, H. Hellsten, and G. Stenstrom, "Synthetic-aperture radar processing using fast factorized back-projection," *IEEE Trans. Aerosp. Electron. Syst.*, vol. 39, no. 3, pp. 760–776, Jul. 2003.
[26] C. Gu, W. Chang, "An efficient geometric distortion correction method for SAR video formation," in *Proc. 5th Int. Conf. Modern Circuits Syst. Technologies*, May 2016.
[27] W. Chang, J. Li, and Z. Zhao, "Consecutive images formation for airborne SAR," in *Proc. IEEE CIE Int. Conf. Radar*, Oct. 2011.
[28] S. Palm and A. Wahlen, "Real-time onboard processing and ground based monitoring of FMCW-SAR videos," in *Proc. 10th Eur. Conf. Synthetic Aperture Radar*, Jun. 2014.
[29] S. Liu and Y. Yan, "A single-channel SAR-GMTI algorithm based on sub-apertures and FrFT," in *Proc. Second Int. Conf. Spatial Inf. Technol.*, Nov. 2007.
[30] D. Pastina and G. Battistello, "Change detection based GMTI on single channel SAR images," in *Proc. 7th Eur. Conf. Synthetic Aperture Radar*, Jun. 2008.
[31] L. Jian and Z. Running, "An efficient image formation algorithm for spaceborne video SAR," in *Proc. IEEE Int. Geosci. Remote Sens. Symp.*, Jul. 2018.
[32] H. Yan and X. Mao, "Frame rate analysis of video synthetic aperture radar (ViSAR)," in *Proc. Int. Symp. Antennas Propag.*, Oct. 2016.
[33] C. K. Kim and S. O. Park, "A modified stripmap SAR processing for vector velocity compensation using the cross-correlation estimation method," *J. Electromagn. Eng. Sci.*, vol. 19, no. 3, pp. 159–165, Jul. 2019.
[34] K. Ouchi, "On the multilook images of moving targets by synthetic aperture radars," *IEEE Trans. Antennas Propag.*, vol. AP-33, no. 8, pp. 823–827, Aug. 1985.
[35] D. E. Wahl and P. H. Eichel, "Phase gradient autofocus-a robust tool for high resolution SAR phase correction," *IEEE Trans. Aerosp. Electron. Syst.*, vol. 30, no. 3, pp. 827–835, Jul. 1994.

Chul Ki Kim was born in Gang-neung, Korea, in July 1989. He received the B.S. degree in electronic engineering from Soongsil University, Seoul, Korea, in 2014, the M.S. degree in electrical engineering from Korea Advanced Institute of Science and Technology, Daejeon, in 2016, and is currently working toward the Ph.D. degree in electrical engineering at Korea Advanced Institute of Science and Technology (KAIST).

His current research interests include Radar system design, Synthetic Aperture Radar (SAR), and Electromagnetics.

Muhammad Tayyab Azim was born in Pakistan, in May 1987. He received the B.E. degree in avionics engineering from NUST, Pakistan, in 2009, and the M.S. degree in electrical engineering from the University of Surrey, in 2011, and is currently working toward the Ph.D. degree in electrical engineering at Korea Advanced Institute of Science and Technology (KAIST). His research interests include electromagnetics, antenna design and microwave components design.

Ashish Kumar Singh (Member, IEEE) received the B.Tech. degree in electronics and communication engineering from Madan Mohan Malaviya University of Technology, Gorakhpur, India, in 2008, the diploma in embedded system design from Centre for Development of Advanced Computing (CDAC), Noida, India, in 2009, and the M.Tech. degree in electronics and communication engineering from Haldia Institute of Technology, Haldia, India, in 2012.

He received the Ph.D. degree in mechatronics from Gwangju Institute of Science and technology (GIST), Gwangju, Korea, in 2018. Currently, he is a Postdoctoral Researcher at the Korea Advanced Institute of Science and Technology, Daejeon, Korea. His current research interests include radar signal processing, FPGA based signal generation and processing, beamforming, and radar system design.

Seong-Ook Park (Member, IEEE) was born in KyungPook, Korea, in December 1964. He received the B.S. degree from KyungPook National University, Korea, in 1987, the M.S. degree from the Korea Advanced Institute of Science and Technology, Daejeon, Korea, in 1989, and the Ph.D. degree from Arizona State University, Tempe, in 1997, all in electrical engineering.

From March 1989 to August 1993, he was a Research Engineer with Korea Telecom, Daejeon, working with microwave systems and networks. He later joined the Telecommunication Research Center, Arizona State University, until September 1997. Since October 1997, he has been with the Information and Communications University, Daejeon, and currently as a Professor at the Korea Advanced Institute of Science and Technology. His research interests include mobile handset antenna and analytical and numerical techniques in the area of electromagnetics.

Dr. Park is a member of Phi Kappa Phi.